

# Transparent Malware Detection With Granular Assembly Flow Explainability via Graph Neural Networks

Griffin Higgins, Roozbeh Razavi-Far, *Senior Member, IEEE*, Hossein Shokouhinejad, and Ali A. Ghorbani, *Senior Member, IEEE*

**Abstract**—As malware continues to become increasingly sophisticated, threatening, and evasive, malware detection systems must keep pace and become equally intelligent, powerful, and transparent. In this paper, we propose Assembly Flow Graph (AFG) to comprehensively represent the assembly flow of a binary executable as graph data. Importantly, AFG can be used to extract granular explanations needed to increase transparency for malware detection using Graph Neural Networks (GNNs). However, since AFGs may be large in practice, we also propose a Meta-Coarsening approach to improve computational tractability via graph reduction. To evaluate our proposed approach we consider several novel and existing metrics to quantify the granularity and quality of explanations. Lastly, we also consider several hyperparameters in our proposed Meta-Coarsening approach that can be used to control the final explanation size. We evaluate our proposed approach using the CIC-DGG-2025 dataset. Our results indicate that our proposed AFG and Meta-Coarsening approach can provide both increased explainability and inference performance at certain coarsening levels. However, most importantly, to the best of our knowledge, we are the first to consider granular explainability in malware detection using GNNs.

**Index Terms**—Malware Detection, Explainability, Graph Neural Network, Assembly.

## I. INTRODUCTION

**M**ALWARE is software explicitly designed with malicious intent for the purposes of disrupting digital information and information systems. The use of machine learning (ML) and deep learning (DL) to automatically detect malware has proven extremely promising. This is especially true for graph learning-based methods that operate on graph data extracted from program flow [1]. However, since GNNs are not *intrinsically explainable*, explanation methods must be used to derive explanations related to a particular prediction. While different types of explanations are possible, extracting an explanatory subgraph related to graph classification (e.g., malware detection) is of special interest to improve model transparency. Such a subgraph can guide our understanding of which underlying phenomenon is influential to a given prediction (i.e., malicious behavior). Subgraph explanations can also help confirm that an underlying prediction, irrespective of correctness, is being made in a non-spurious manner. Most importantly, the task of malware detection also demands heightened transparency as the cost of false negative predictions or misleading explanations are extremely high.

Building on this, it is also important to assess the explanation *quality* for a given subgraph. This can be viewed and measured

in two fundamental ways. Specifically, an explanation subgraph can be either *sufficient*, where the extracted subgraph matches the prior prediction of the model on the original sample or *necessary* where the original sample with the subgraph removed generates a different prediction from the prior models prediction on the original sample. However, when evaluated together, an explanatory subgraph that is able to achieve both a highly necessary and sufficient explanation gives rise to a further notion of a highly *characterized* explanation [2]. This is similar to the way that F1 score provides a deeper understanding of classwise performance with respect to both precision and recall.

Furthermore, it is important to also consider explanation *granularity*. While prior works have considered GNN malware explainability on CFGs, a key limitation is that they are ultimately unable to provide highly characterized instruction level subgraph explanations. This is not a limitation of GNNs or methods per se, but rather of the underlying CFG graph structure. In a CFG, nodes are represented as sequences of non-branching assembly instructions, formally referred to as basic blocks, that are directly connected to other nodes by edges that represent branching (e.g., jump instructions). However, since the instructions do not play an observable role in the CFG graph structure they therefore cannot be explained via GNNs. Additionally, since basic blocks may contain many assembly instructions it becomes ambiguous as to which instructions contribute to the explained behavior. By comparison, granular instruction level explanations are superior and needed since they can provide unambiguous explanations needed to enhance model transparency. While some related works do consider aspects of instruction level program flow via opcode graphs as Markov chains [3], [4], [5], [6], [7], [8], [9], our work is distinct and novel since we consider the assembly instruction level flow of an entire program as a graph, that we term Assembly Flow Graph (AFG). In our work, we use AFG to improve detection performance and strongly characterize the predicted behavior of a sample through the use of GNNs. This approach is important because it can provide granular explanations to help understand and characterize malware behavior. This is especially useful for assisting malware analysis where the number of instructions are large.

However, many challenges related to the large size and scale of AFGs make most aspects of applying GNNs (preprocessing, embedding, training, explaining, etc.) non-trivial. To address this, we apply coarsening, a graph reduction technique, to reduce both nodes and edges in the original graph to a prespecified size. Critically, we select coarsening since it aims to maintain structural similarity to the original graph while also

G. Higgins, R. Razavi-Far, H. Shokouhinejad, and A. Ghorbani are with Canadian Institute for Cybersecurity, University of New Brunswick, Fredericton, Canada (e-mail: griffin.higgins@unb.ca).

providing nodewise backtrackingability from reduced to original nodes.

Nonetheless, applying coarsening directly on AFG remains computationally challenging. To alleviate this, we propose Meta-Coarsening, shown at a high level in Fig. 1, where we first coarsen the CFG, (i.e., AFG meta-structure) to approximate coarsening AFG directly. Once a coarsened C-CFG, dataset is constructed a GNN model is then trained and an explainer is used to derive explanations. Here, the most important C-CFG explanation subgraph is then backtracked onto the underlying AFG. Afterwards, an entirely separate backtracked AFG (B-AFG) dataset is used to train a separate GNN model. An explainer is then used to derive the final B-AFG subgraph level explanation *at the assembly instruction level*. This approach has the advantage that any subgraph of the AFG can be arbitrarily examined under a varying level of coarsening and adjusted to fit the computational requirements or explanation expressiveness.

To evaluate our proposed approach, we conduct experiments on the Dynamically Generated Graphs for Malware Analysis (CIC-DGG-2025) [10]. Specifically, we consider several coarsening methods and coefficients and evaluate our work using the strongest available explainability metrics. We also propose several novel metrics to assess quality and granularity of explanations. Importantly, to the best of our knowledge, we are the first to propose granular explainability at the assembly level for malware detection.

In summary, our contributions are as follows:

- We propose a novel program graph type, AFG, to represent the assembly instruction flow of a binary executable.
- We capture granular explainability of AFG towards enhanced GNN transparency.
- We propose a novel Meta-Coarsening approach to improve computational tractability over large graphs.
- We define several novel explanation metrics to quantify explanation granularity and quality.
- We consider several hyperparameters to control the size of explanations.

The remainder of this paper is organized as follows. In Section II we conduct a literature review. In Section III we provide background. Section IV we cover our methodology. In Section V we present our evaluation. In Section VI we discuss the work and note limitations. Lastly, in Section VII, we conclude our work.

## II. LITERATURE REVIEW

In this section, various related works that consider either graph based instruction level malware detection and classification (i.e., excluding CFG level) or contribute to explainable graph based malware detection methods generally are considered.

### A. Opcode graph mining for malware detection and classification.

In [3], the authors propose using support vector machines (SVMs) to detect and classify malware. Initially, all pairs of successive instructions are recorded with observed counts in matrix form. Afterwards, the matrix is normalized to

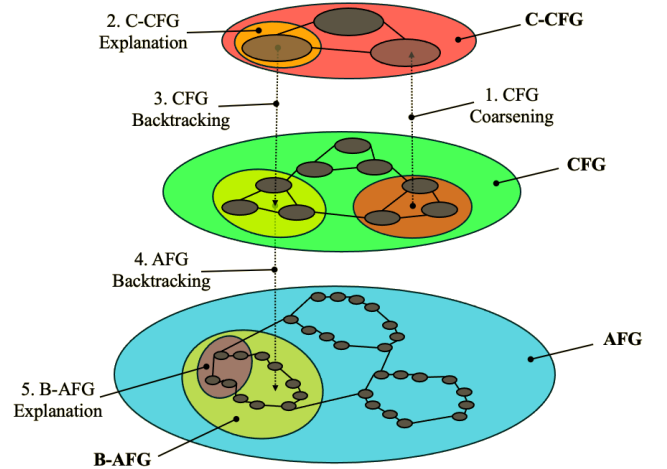


Fig. 1. High-level diagram of our proposed approach with training and embedding phases omitted. CFG and starting point is shown in the middle green patch, coarsened CFG (C-CFG) shown in the top red patch, and AFG is shown in the bottom blue patch. The C-CFG explanation and backtracked AFG (B-AFG) are shown in yellow. The most important B-AFG explanation subgraph is shown in purple.

form a Markov chain where nodes represent instructions and edges represent transition probabilities. Graph kernels are then applied to score the graph and supplied as input to SVMs.

In [4], the authors propose the same initial opcode graph construction approach as [3] but compare the graphs directly instead of applying graph kernels and SVMs. Specifically, the authors propose a score to measure the similarity between two Markov chain opcode graph representations. The score is used to compute similarity between known metamorphic samples to detect matches. The authors set a score threshold to classify a given sample as malicious or benign.

In [5], opcode graphs as in [3], are used and power iteration is used to derive graph embeddings input to an ensemble of classifiers to detect malware. Models such as k-nearest neighbors (KNN), Adaboost, SVM are used in the ensemble.

In [6], Graph Mining for Metamorphic Malware Detection (G3MD) is proposed as an approach to classify metamorphic malware families. The approach adopts the graph construction strategy proposed by [4], [3] and attempts to find frequent subgraphs within malicious metamorphic opcode graphs via graph mining. The subgraphs are then saved as micro-signatures and matched against a given sample. Matches are then vectorized and a classifier is used to classify a given sample as belonging to a given metamorphic malware family.

In [7], the authors propose Higher-level Engine Signature based Metamorphic Malware Identification (HLES-MMI) to identify metamorphic malware. The approach uses a co-opcode graph constructed for each malware family as in [4]. The authors also propose Graph Similarity based Metamorphic Malware Identification method (CGS-MMI) to compare a sample with all co-opcode graphs for each family. Furthermore, the size of the graphs are reduced as to their largest connected component.

In [8], opcode sequences are first extracted from disassem-

bled malicious families and constructed as opcode graphs following [4], [6]. Opcode filtering for low frequency opcodes is also applied to reduce the size of the opcode graph. Afterwards, similarity comparison as proposed in [4] is performed to group malware families. Sub-family clusters are then derived using multi round Density-Based Spatial Clustering of Applications with Noise (DBSCAN). Afterwards, representative sub-family opcode graphs signatures are then used to detect and classify samples that may be polymorphic or metamorphic, or both.

In [9], a Sequential Opcode Embedding-based Malware Detection (SOEMD) approach is proposed that aims to capture opcode sequences through weighted random walks. However, only strongly connected substructures are considered via an edge selection process. Afterwards, a Skip-Gram model is used to embed all walks input as unique one-hot encodings. The authors justify the approach to avoid having long opcode sequences.

### B. Explainable GNN for malware detection and classification.

In [11], a CFGExplainer is proposed to explain GNN-based malware detection at the CFG level. CFGExplainer captures important CFG subgraphs that relate to the prediction of the GNN model. Specifically, malicious attribute CFGs are used to train a GNN model where node attributes are constructed via assembly instruction information to produce initial CFG node embeddings. Furthermore, a two-stage approach is used. Firstly, node embeddings are learned by a model that assigns node embedding scores. Secondly, the assigned learned scores are used to obtain subgraph importance. Several GNN explainers such as GNNExplainer, PGExplainer, and SubgraphX are also evaluated against the proposed CFGExplainer.

In [10], several GNN explainers, namely GNNExplainer, PGExplainer, and CaptumExplainer are considered to evaluate the explainability of GNN-based malware detection. In this work, dynamically generated CFGs are extracted from benign and malicious samples. Nodes in each sample are embedded using assembly instructions before being passed through an auto encoder. Embedded samples are then trained and tested using a standard GCN model. Samples are then explained using the provided explainers and evaluated. A novel explanation selection method, Greedy Edge-wise Composition (GEC), is proposed in place of Top-Edge Selection (TES) to address the problem of having many disconnected subgraphs at various levels of selection sparsity. Furthermore, a novel explainer, RankFusion, is proposed to aggregate and improve explanations from multiple high performing explainers.

In [12], a dual explainability framework is proposed that considers GNN-based malware detection subgraph explanations. Specifically, as in [10], dynamically generated CFGs are extracted from benign and malicious samples and embedded. Several GNN models such as GCN, GAT, and GraphSAGE are then trained and tested. Furthermore, three GNN explainers, Integrated Gradients, Guided Backpropagation, and Saliency, are used to extract important subgraphs signatures from benign and malicious samples and build a verified query box. When evaluating a unseen sample signatures in the query box are tested for subgraph isomorphic or monomorphic matches

within the unseen sample graph through an approach termed SubMatch.

In [13], a survey of recent advances in malware detection and explainability with GNNs is provided. Emphasis is placed on malware analysis and datasets, graph reduction strategies, and GNN explainability are covered.

## III. BACKGROUND

Here we cover background needed to understand different aspects of our work. Specifically, we provide information on our sample focus area, Windows PE files, as well as CFGs, coarsening, GNNs, and GNN explainability.

### A. Windows PE

The Portable Executable (PE) file format is a specification used by Windows operating systems to describe the architecture of executable files, and object files referred to as PE and Common Object File Format (COFF), respectively. Of course, the executable is portable, meaning it can run on many different hardware architectures, such as x86-32. The PE executable format is organized with the MS-DOS Header, MS-DOS Stub, PE Header, Section Headers, and Image Pages. Many other subsections (e.g., .data and .text) are equally important for the functioning of the format. For a comprehensive review of the PE file format please see [14]. Most importantly, since the PE format exists as part of (currently) the most dominant consumer facing operating system, i.e., Windows. As such, it is entirely reasonable to expect an adversary to target the PE format in order to indirectly perpetrate harm against consumers generally.

### B. Control Flow Graphs

CFGs are graph data representing an abstracted view of program by considering nodes as sequences of non-branching assembly instructions. Therefore, any type of branching can be represented by an edge to another basic block. Importantly, nodes can contain many types of data related to it apart from the assembly instructions themselves.

### C. Graph Coarsening

Graph coarsening is one of several existing categories of graph reduction techniques, which aim to reduce the size of a graph via the contraction of disjoint sets of connected nodes into supernodes. Importantly, during contraction the overall graph retains a similar representative topology or structure as the original. This is distinct from other related graph reduction techniques such as sparsification and condensation, since information is not necessarily synthesized or removed. Instead, all information is still entirely backward referential since a surjective mapping between nodes in the original and coarsened levels are maintained. This means that given a coarsened graph it is possible to backtrack supernodes, and hence subgraphs, to the original graph, so long as the original graph structure is known so an edgewise subgraph can be induced. Lastly, coarsening methods also allow for coarsening to a specific size as specified by the  $r$  coarsening coefficient. Specifically, the coefficient reduces a graph to  $1 - r$  of its original size.

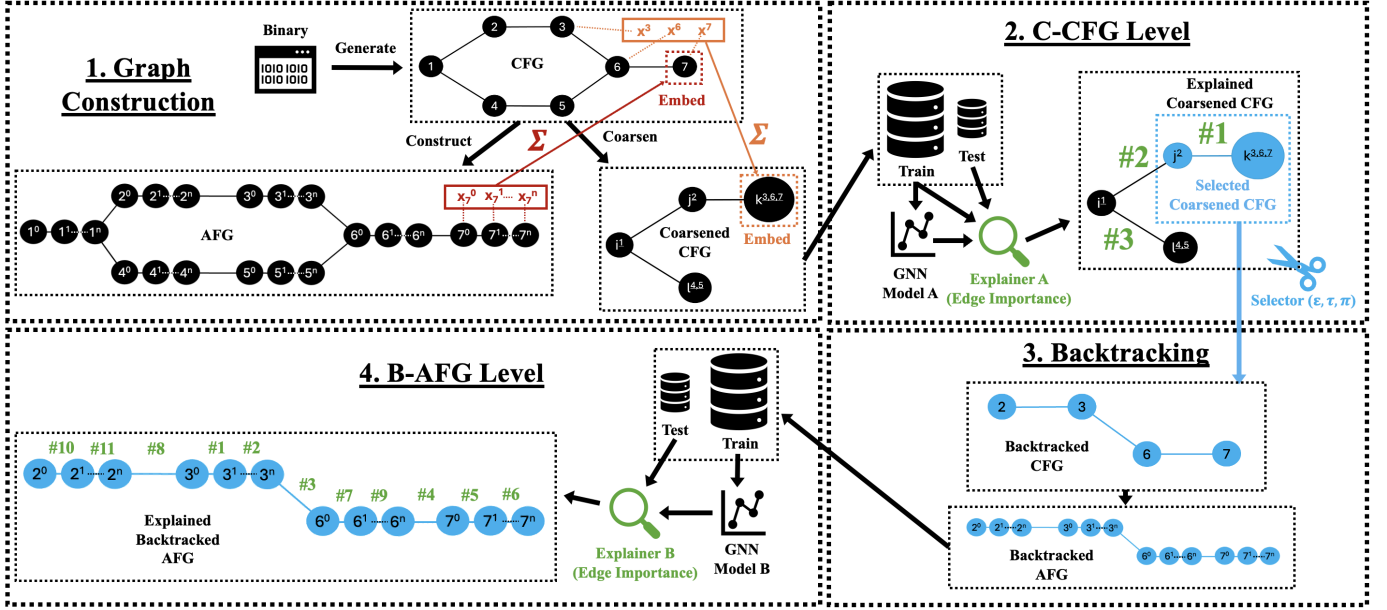


Fig. 2. Detailed diagram showing four phases of processing.

#### D. Graph Neural Networks

GNNs operate on attribute graph-structured data to learn high dimensional representations for graph primitives towards a specific task. Here, tasks can range in level, from nodes and edges to subgraphs and graphs. Additionally, tasks may be supervised (e.g., classification or regression), unsupervised (e.g., clustering), or semi-supervised.

Formally, the input GNN takes the form  $\mathcal{G} = (\mathcal{V}, \mathcal{E})$ , where  $\mathcal{E}$  represents the edge list (or adjacency matrix similarly) and  $\mathcal{V}$  represents the set of nodes or vertices. We opt for the former term. Importantly, in an attribute graph nodes are assigned attribute vectors, i.e., message initializations, stored in  $\mathbf{X} \in \mathbb{R}^{n \times d}$  of the form  $\mathbf{x}_v \in \mathbb{R}^d$ , where  $n$  is the number of nodes,  $d$  is the attribute vector dimension, and  $v$  is a node in  $\mathcal{V}$ . These initialized message vectors are then updated, and learned by GNNs during training, via message passing between neighboring nodes. The exact neighborhood is defined through the function  $\mathcal{N}$ . Additionally,  $l$  layers, or rounds, of message passing are performed where neural networks optimize the final attribute vectors for each node. The generalization of this process takes the form:

$$\mathbf{x}_v^{(l)} = \gamma^{(l)} \left( \mathbf{x}_v^{(l-1)}, \bigoplus_{u \in \mathcal{N}(v)} \phi^{(l)}(\mathbf{x}_v^{(l-1)}, \mathbf{x}_u^{(l-1)}) \right) \quad (1)$$

Here,  $\bigoplus$  is a permutation invariant aggregation function (e.g., sum, mean, or max). Furthermore,  $\phi$  and  $\gamma$  are differentiable functions used to update messages. Edges may also optionally contribute to a message update with separate input information, however we do not consider this here.

#### E. GNN Explainability

GNN explainability methods can fall into two categories: factual and counterfactual. In factual methods, the target is to

identify the components of the input graph that directly affect the GNN model's prediction. These components comprise information about nodes, edges, and node features that GNN models use during message passing and prediction. On the other hand, Counterfactual explanation methods pinpoint how a minimal perturbation of the input graph could change the model prediction and describe how sensitive it is to graph structure or to node features.

GNN explainers can be divided into post-hoc and self-interpretable approaches, depending on their architecture. Post-hoc explainers leverage the trained model to produce explanations either via black-box or white-box techniques while self-interpretable explainers integrate the explanation mechanism within the GNN model design. Indeed, self-interpretable explainers rely on information-theoretic or structural constraints to highlight an important subgraph used for both prediction and explanation tasks.

Also, explanations can be classified into two main categories in terms of the scope of analysis: instance-level and model-level explanations. Instance-level explainers generate interpretations based on a specific input graph and provide localized insights into individual predictions. Model-level explainers aim to determine the overall decision-making behavior of the GNN model, seeking broader patterns that likely hold across the majority of inputs [13].

## IV. METHODOLOGY

Here, we present our proposed Meta-Coarsening approach covering all phases as shown in Fig. 2. In Section IV-A we first describe phase 1, the initial graph construction process in for CFG, AFG, and C-CFG graphs. Importantly, while the CFG generation process must proceed the AFG and C-CFG construction that latter two graph can be constructed independently from the CFG. Additionally, we also describe the instruction encoding process used in the work. Next, in

Section IV-B, we consider the operations related to the C-CFG level of our proposed approach. Specifically, we cover the training and explaining of C-CFGs as well as the selection of explanation needed for the backtracking stage. In Section IV-C, we describe the backtracking process to reach the B-AFG and the difference in embedding used as compared to C-CFG. Lastly, In Section IV-D, we finish with a brief description of the training and explanation process to reach the final instruction level explanation.

### A. Graph Construction

1) *CFG Generation*: We begin by first obtaining attribute CFGs of benign and malicious Windows PE x86 executable samples. Here, we consider CIC Dynamically Generated Graphs for Malware Analysis (CIC-DGG-2025) [10], discussed further in Experimental Setup. angr Python library (version 9.2.89) to dynamically generate CFGs. angr leverages symbolic execution and constraint solving to recover program flow and CFGs [15], [16], [17]. angr also relies on various libraries such as capstone for instruction encoding that we use to derive instruction features in our work. The resulting CFG can be used to access the assembly instructions, and other information, located within each CFG node to construct the AFG, discussed hereafter. Lastly, the embeddings for CFG nodes are simply the sum of all instruction encoding that belong to them, as shown in Fig. 3.

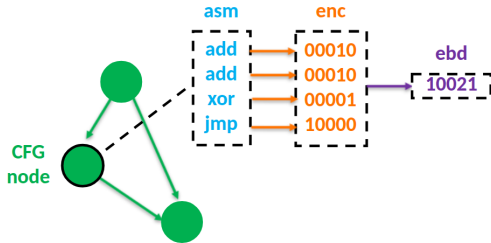


Fig. 3. CFG embedding procedure.

2) *AFG Construction*: Given a CFG, captured dynamically from a Windows PE x86 executable binary, as is the case for CIC-DGG-2025 [10], we construct an AFG, as shown in Fig. 4, by substituting all CFG nodes, i.e., basic blocks, with their respective non-branching sequential assembly instructions. Such instructions can be represented as a singly linked list, that we refer to hereafter as the *instruction list* for a given CFG node. Importantly, all incoming edges to the original CFG node are reassigned to the respective instruction list head node and all outgoing edges from tail node.

3) *CFG Coarsening*: Due to the large size of many AFGs, the direct application of coarsening often becomes computationally intractable or extremely costly in practice. To address this, we propose to instead coarsen the CFG which is computationally tractable to produce a C-CFG. In our work, we utilize the coarsening library from [18]. Specifically, we aim to take the advantage of the hierarchical relationship between the various levels of granularity and backtrack explanations from

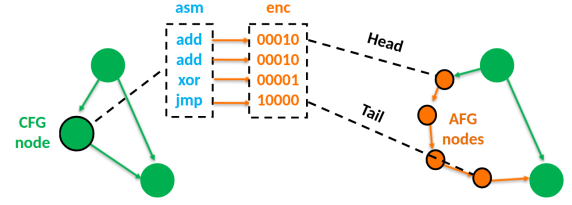


Fig. 4. AFG construction and embedding procedure for one node.

C-CFG supernodes to CFG basic block nodes and eventually to AFG instructions nodes. We argue that coarsening the CFG, to approximate coarsening the underlying AFG is reasonable. This is partially owing to the computational tractability of coarsening a CFG, but mainly due to the *guaranteed* structural similarity between CFG and AFG. By this, we simply mean that that nodes in CFG with specific in and out degrees are guaranteed to retain their respective in and out degrees in the AFG, just at opposite ends of the substituted instruction list. Otherwise, apart from the increase in nodes the general structure of AFG remains well constrained by its respective CFG. Moreover, it is also guaranteed that only path graphs or linked lists will be substituted in place of CFG nodes rather than highly complex and unpredictable graph structures. To compute the embedding of each C-CFG supernode we simply sum the embeddings of all contracted CFG nodes, whose embeddings are the sum of all instruction encodings that belong to them.

TABLE I  
INSTRUCTION FEATURES AND DIMENSION FOR NODE EMBEDDING.

Feature	Dim	Feature	Dim
prefix <sub>0</sub>	2	xop cc	5
prefix <sub>1</sub>	4	sse cc	21
prefix <sub>2</sub>	7	avx cc	1
prefix <sub>3</sub>	2	avx sae	1
opcode <sub>0</sub>	200	avx rm	5
opcode <sub>1</sub>	191	eflags	1
opcode <sub>2</sub>	37	fpu flags	1
opcode <sub>3</sub>	1	modrm offset	10
rex	17	disp offset	12
addr size	3	disp size	5
modrm	256	imm offset	10
sib	255	imm size	5
sib scale	21		

4) *Instruction Encoding*: For encoding instructions we consider the most representative and variable categorical feature subset, shown in Table I, of a given instruction node, generated by the capstone library [19] angr [15], [16], [17]. Additionally, we consider the prior frequency of all well defined categorical features across the millions of instructions in our training set (derived from hundreds of samples across independent datasets). Specifically, we observe that while many one-hot encoding categories are reserved many are not observed in training. Thus, we can save one-hot encoding space by only considering observed categories and remapping them to a reduced one-hot space. However, for each category, we include an additional bit for each feature to capture the unlikely occurrence of out of vocabulary instruction level categories for the reduced one hot mapping with respect to our dataset. In total, we consider

a 1076 dimensional vector with additional 27 bits of out of vocabulary space, bringing the total to 1103 bits.

### B. C-CFG Level

1) *(C-)CFG Training and Explaining*: During the training phase a GNN model is selected and trained on the embedded (C-)CFG training graphs and tested on the test graphs. Its weights are then saved for future use with respect to explanation and further evaluation. Once training is completed an explainer is selected and each test sample is explained using the GNN model, prediction, and test sample as input. The returned output from the explainer are the corresponding set of edge importance weights (C-)CFG.

2) *(C-)CFG Selection*: After a given explanation is provided for a specific (C-)CFG sample, a subgraph must be selected according to a given selection algorithm  $\tau$  e.g., Top Edge Selection, and selection policy  $\pi$ , e.g., keep 5 percent of the top nodes. Together, a final subgraph explanation can be provided at the (C-)CFG level and used in the next phase for backtracking to the AFG.

### C. Backtracking

1) *(B-)AFG Construction*: Using the prior C-CFG subgraph explanation a AFG subgraph can be backtracked and defined through the mapping between supernodes in the (C-)CFG, basic block node in the CFG, and instruction nodes in the AFG. Once the B-AFG subgraph is defined embeddings for each node are computed. However, unlike the prior embedding of the (C-)CFG, (B-)AFG embedding cannot rely on an aggregated embedding representation to reduce its memory footprint. Instead, each node exists in its pure unaggregated form. This is an attractive property for explainability but raises computational concerns from a space perspective since AFGs may be very large compared to CFGs. Therefore, it is worthwhile to consider our prior feature selection for (C-)CFGs and opt for a reduced feature or feature subset. Here, we only consider the single reduced opcode<sub>0</sub> feature of 201 dimensions including the one out of vocabulary bit. This feature is specifically selected since it can capture the operations being performed at the assembly level while enabling backtracking over larger B-AFG subgraphs needed to obtain improved Fidelity+ score, discussed in Section V-B.

### D. B-AFG Level

1) *B-AFG Training and Explaining*: After all B-AFGs are constructed and embeddings are computed, a completely new GNN model is used and trained on the B-AFG graphs. Additionally, only after the (C-)CFG model is fully trained and B-AFG graph are defined can the B-AFG model begin training. After training is concluded the test samples can then be explained using an explainer. Lastly, granular explanations at the instruction level can be provided and subsequently assessed.

## V. EVALUATION

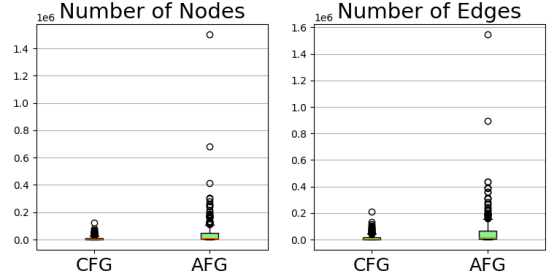
In our work, we evaluate several relationships between *coarsening*, *inference*, and *explainability* as applied to our

novel Meta-Coarsening approach. Specifically, we formulate the following research questions:

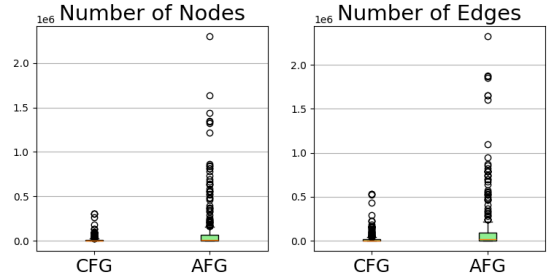
- **RQ1**: Is the application of *coarsening* harmful or helpful for improving *inference* performance with respect to coarsening method and coefficient on average accuracy?
- **RQ2**: Is the application of *coarsening* harmful or helpful for improving *explainability* with respect to coarsening method and coefficient on  $\lambda$  score (introduced in Section V-B)?
- **RQ3**: Are there any noticeable *classwise differences* or *trends* with respect to *inference* or *explainability*?

### A. Experimental Setup

1) *Dataset*: In this work, we consider the CIC-DGG-2025 [10] dataset that provides our initial attribute CFGs across two datasets, namely, DikeDataset [20] and PE Malware Machine Learning Dataset (PMMLD) [21]. Here, benign samples belong exclusively to the DikeDataset and malicious samples belong exclusively to PMMLD dataset.



(a) DikeDataset sample sizes in nodes and edges (benign).



(b) PE Malware Machine Learning Dataset sample sizes in nodes and edges (malicious).

Fig. 5. Size comparison of datasets with respect to CFG and AFG number of nodes and edges.

Furthermore, we consider a stratified classwise, but not dataset wise, train test split of 80% between all non-isomorphic CFGs samples in the dataset with 45% benign and 55% malicious samples. We fix the training and test sets for all models and experiments in our work. Additionally, the frequency of all well-defined categorical features (e.g., opcode) are recorded for each training sample to construct the instruction encoding discussed prior. Next, we proceed to construct the full AFG for each remaining CFG. The size, in number of nodes and edges, for each dataset is shown in Fig. 5. Importantly, a very large difference between CFGs and AFGs can be observed helping to motivate the application of coarsening due to the large size

difference between nodes and edges in CFGs and AFGs in each dataset.

2) *GNN Model and Hyperparameters*: In our work, we train 18 Graph Convolutional Network (GCN) [22] models. All models are provided with the same training configuration, namely, three layers, 50% dropout, input dimension equal to the length of the (C-)CFG/B-AFG node attribute vector, hidden dimension of 128, output dimension of 2. Furthermore, for the optimizer we utilize Adam with a learning rate of 0.001. In terms of loss function, we use the Cross Entropy (CE) loss. Lastly, we train our models for 150 epochs with a fixed batch size of 8. After training is complete, we consider the model with the lowest validation loss for evaluation.

*GNN Explanation and Hyperparameter Selection*: In our work, we consider the Integrated Gradients (IG) explainer provided by the Captum library [23]. We also provide additional explainability comparison with other captum explainers in Appendix A. However, while other explainers, such as GNNExplainer [24] and PGExplainer [25] are capable of node level explanations, other works have observed that such explanations are not as consistent or high quality as the former in a similar setting to ours [10] and are not considered further. Additionally, we define  $\pi$ , i.e., selection stopping policy, as the selection of ranked edges, output from a given selection method  $\tau$ , up to a percentage  $\epsilon$  of nodes in the original graph, selected as a edgewise subgraph of the original graph. If the percentage is less than the number of nodes in the graph we simply select the maximum of either the logarithmic number of nodes in the graph or one edge. This guarantees that a non empty graph is always selected. Furthermore, we define the unimportant subgraph as the edgewise subgraph of the original graph, for all non-important edges. We fix our chosen  $\epsilon$  value at 0.10 for all experiments. Furthermore, we choose TES as our  $\tau$  selection method.

3) *Coarseners*: In our work, we select the Kron reduction method [26] that adapts a Laplacian pyramid transform for graph signals using downsampling, reduction, spectral filtering, and interpolation operations on graphs to approximate the underlying graphs. While technically not a coarsening method [18], it is able to reduce the graph by a factor of two at each level and maintain the effective resistance distance. While Kron has many drawbacks it enables certain theoretical guarantees that make it popular as a coarsening method. Additionally, we also select the edge variant of the local variation coarsening method (Variation Edges) [18] that relies on restricted spectral approximation and greedy algorithms that operated on small well-connected sets and select those with minimal local variation. The approach achieves improved performance over coarsening methods such as Kron. However, other coarsening methods are available such as heavy edge, neighborhood local variation, algebraic distance, and affinity. Thought, we do not consider them simply to limit the large scope of our existing experimental setting.

4) *Hardware and Software*: In our work, we use Intel Xeon Platinum 8253 (32) @ 3.000GHz and 128GB of memory with NVIDIA Quadro RTX 6000/8000 as well as a Xeon Silver 4114 (20) @ 3.000GHz and 64GB of memory with two NVIDIA TITAN V's. Furthermore, we utilize Python version 3.12.9 and

extensively utilize the PyTorch Geometric graph representation deep learning library [27], [28], Networkx [29], as well as angr and its modules such as capstone [15], [16], [17].

## B. Metrics

1) *Inference Metrics*: In terms of evaluation metrics, it is important to separate the (C-)CFG and B-AFG inference and explainability performance since they represent entirely separate models. However, the B-AFG model is dependent on the (C-)CFG model and chosen explainer module (*explainer*,  $\tau$ , and  $\pi$ ) for defining its training and testing B-AFG datasets. Additionally, since different  $r$  values can produce different (C-)CFG and B-AFG sizes they must also be considered. We use the standard accuracy, precision, recall, and F1 score. Specifically, TP is true positive, TN is true negative, FP is false positive, and FN is false negative, formulated below as:

$$\text{Accuracy} = \frac{TP + TN}{TP + TN + FP + FN} \quad (2)$$

$$\text{Precision} = \frac{TP}{TP + FP} \quad (3)$$

$$\text{Recall} = \frac{TP}{TP + FN} \quad (4)$$

$$\text{F1 score} = \frac{2 \cdot \text{Precision} \cdot \text{Recall}}{\text{Precision} + \text{Recall}} \quad (5)$$

2) *Explainability Metrics*: To assess explainability performance, we use the standard Fidelity+ ( $fid_+$ ) and Fidelity- ( $fid_-$ ) scores where higher  $fid_+$  and lower  $fid_-$  scores are preferred, respectively.

$$fid_+ = 1 - \frac{1}{N} \sum_{i=1}^N \mathbb{1}(\hat{y}_i^{G_{C \setminus S}} = \hat{y}_i) \quad (6)$$

$$fid_- = 1 - \frac{1}{N} \sum_{i=1}^N \mathbb{1}(\hat{y}_i^{G_S} = \hat{y}_i) \quad (7)$$

$$\mathbb{1}(x) = \begin{cases} 1 & \text{if } x > 0 \\ 0 & \text{if } x = 0 \\ -1 & \text{if } x < 0 \end{cases} \quad (8)$$

Here,  $\hat{y}_i$  is the prior prediction on a given sample  $s$ ,  $\hat{y}_i^{G_{C \setminus S}}$  is the prediction of  $s$  with the important subgraph removed, and  $\hat{y}_i^{G_S}$  is the prediction of  $s$  considering only the important subgraph. Since our task is classification and not regression, we express the fidelity scores using indicator functions  $\mathbb{1}$ , also referred to as accuracy, ( $fid_{+/-}^{acc}$ ) over predicted probabilities ( $fid_{+/-}^{prob}$ ) as mentioned in [2].

3) *Lambda Score*: The characterization score ( $character$ ) is the weighted harmonic mean of  $fid_+$  and  $fid_-$ , i.e., same as Micro-F1 for precision and recall, where  $w_+$  and  $w_- \in [0, 1]$  and where  $w_+ + w_- = 1$ . We assign  $w_+ = w_- = 0.5$  as shown below:

$$character = \frac{w_+ + w_-}{\frac{w_+}{fid_+} + \frac{w_-}{1 - fid_-}} \quad (9)$$

Furthermore, we recognize that a “good” characterization score to be 0.6 based on different experimental settings as conducted and proposed in [2]. The reason for this is that high  $fid_+$  scores near 1 are extremely difficult to achieve compared to  $fid_-$  scores near zero. Therefore, we also consider this as the preferred upper bound in a non-trivial setting.

However, while the characterization score is one of the strongest available explanation evaluation metrics it does not consider the contextual relationship between the selected (C-)CFG and B-AFG. Instead, it only considers the context independent explainability of a given graph. Specifically, the fact that it may be a related or important subgraph from a prior explanation is not considered. Therefore, we argue that any “re-characterization” of a highly characterized subgraph ought to be especially difficult to obtain by definition. That is, a high characterization score is indicative of a selected subgraph that is both sufficient and *necessary*. Therefore, if the subgraph were observed to be highly characterized and then individually re-characterized with a similarly high value this would serve as a contradiction. As such, we propose a level aware  $\lambda$  explainability score that aims to capture the level of explanation agreement as the difference between the (C-)CFG and B-AFG levels. Here, a higher value is better, and a negative value is especially unacceptable.

$$\lambda = character_{(C-)CFG} - character_{AFG} \quad (10)$$

4) *Beta Score*: Furthermore, we also recognize that explanations made at the (C-)CFG level are not able to attribute importance at the instruction assembly level. This is by definition since nodes that compose (C-)CFGs are represented as basic blocks or similar, i.e., they consist of multiple instructions that in our case are aggregated via a permutation invariant function (e.g., sum, mean, max, etc.). Importantly, this aggregation is one way, such that an explanation cannot be attributed to an individual instruction post explanation. To capture this, we propose a novel metric, called  $\beta$  indicator score, that outputs a ratio value for a set of samples indicating the degree of instruction level explainability.  $\beta$  returns 0 if all test samples contain binary values and a positive value if any vectors contain non-binary values. If all samples contain non-binary values  $\beta$  is 1.

$$\beta = \frac{\sum_{i=1}^n \text{sgn}\left(\sum_{j=1}^m |x_{ij}(1 - x_{ij})|\right)}{n} \quad (11)$$

We report the  $\beta$  value for all test samples to show if any explanations on any test sample at the (C-)CFG level can be used to attribute importance at the assembly level. At the B-AFG level  $\beta$  is expected to be 0. We stress the importance

and novelty of this metric since it empirically demonstrates the level of explanation granularity of any method specific to our setting.

### C. Inference Evaluation

When examining general trends over all experiments at both the (C-)CFG and B-AFG levels, shown in Table II, we note that most models generally achieve moderate to good performance (F1 score generally between 85-90%) in terms of both positive and negative F1 scores (malicious and benign, respectively). However, consistent under performance of the benign class can be observed across all experiments. This may be due to the ratio of malicious to benign samples, roughly 1.2 times as many.

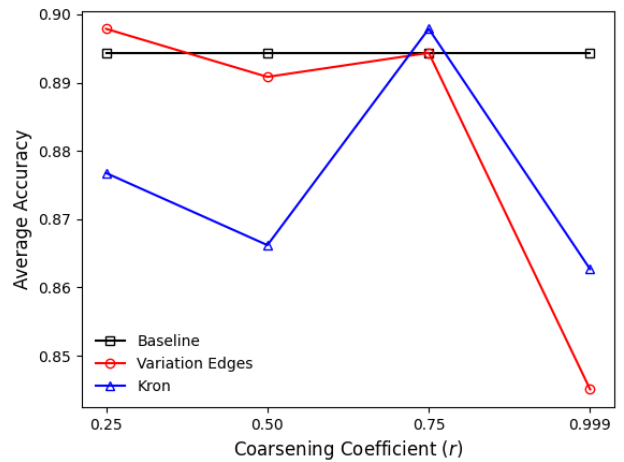


Fig. 6. Meta-Coarsening average accuracy.

When assessing inference performance of our Meta-Coarsening approach holistically, shown in Fig. 6, we consider the average accuracy of both C-CFG and B-AFG levels together. Here, we observe that both coarsening methods decline from low to mild ( $r$  of 0.25 to 0.50) coarsening, increase from mild to moderate coarsening ( $r$  of 0.50 to 0.75), and significant drop from moderate to maximal coarsening ( $r$  of 0.75 to 0.999). Furthermore, we observe that Variation Edges is consistently closer to the baseline than Kron. The best performance of 89.8%, **+0.4** over the baseline, is achieved by both Kron and Variation edges with  $r$  values of 0.25 and 0.75, respectively. However, we recognize that Kron is better since it achieves the best performance at a higher coarsening level making it more computationally efficient for GNN training and explanation. 25% CFG size compared to 75% CFG size in the case of Kron. Overall, this aligns with our intuition that coarsening may act to regularize samples and make it easier for a GNN model to generalize. However, with respect to **RQ1**, certain coarsening methods and coefficients can be more beneficial for inference performance than others and improve over the baseline.

When assessing the performance of each level individually, shown in Table II, the highest C-CFG level accuracy is achieved by Variation Edges with  $r$  of 0.75 with 92.3% accuracy, **+2.2%**

TABLE II  
INFERENCE RESULTS.

Method	$r$	Level	Inference								
			Average Accuracy	Accuracy	F1 score		Recall		Precision		
					Benign	Malicious	Benign	Malicious	Benign	Malicious	
Baseline	0	CFG	0.894	0.901	0.896	0.907	0.938	0.872	0.857	0.944	
		B-AFG		0.887	0.882	0.892	0.938	0.846	0.833	0.943	
Variation Edges	0.25	C-CFG	<b>0.898</b>	0.894	0.884	0.903	0.891	0.897	0.877	0.909	
		B-AFG		0.901	0.894	0.908	0.922	0.885	0.868	0.932	
	0.5	C-CFG	0.891	0.901	0.883	0.915	0.828	0.962	0.946	0.872	
		B-AFG		0.880	0.864	0.893	0.844	0.910	0.885	0.877	
	0.75	C-CFG	0.894	0.923	0.917	0.927	0.953	0.897	0.884	0.959	
		B-AFG		0.866	0.861	0.871	0.922	0.821	0.808	0.928	
	0.999	C-CFG	0.845	0.810	0.803	0.816	0.859	0.769	0.753	0.870	
		B-AFG		0.880	0.866	0.892	0.859	0.897	0.873	0.886	
	Kron	0.25	C-CFG	0.877	0.880	0.870	0.889	0.891	0.872	0.851	0.907
			B-AFG		0.873	0.862	0.883	0.875	0.872	0.848	0.895
0.5		C-CFG	0.866	0.880	0.876	0.884	0.938	0.833	0.822	0.942	
		B-AFG		0.852	0.847	0.857	0.906	0.808	0.795	0.913	
0.75		C-CFG	<b>0.898</b>	0.894	0.882	0.904	0.875	0.910	0.889	0.899	
		B-AFG		0.901	0.892	0.909	0.906	0.897	0.879	0.921	
0.999		C-CFG	0.863	0.831	0.818	0.842	0.844	0.821	0.794	0.865	
		B-AFG		0.894	0.878	0.907	0.844	0.936	0.915	0.880	

over the baseline. Furthermore, the best B-AFG level inference performance is achieved by both Kron and Variation Edges at  $r$  values of 0.25 and 0.75, respectively, that achieve 90.1% accuracy, **+1.4%** over the baseline. This slight drop in inference performance between the C-CFG and B-AFG levels matches our intuition since B-AFG graphs are more variable and contain less information compared to the (C-)CFG level. With respect to individual coarsening trends generally, we observe an increase in performance at the C-CFG level for both methods as coarsening is increased, and, then, a significant drop once maximal coarsening is reached. This suggests that a coarsening threshold exists where samples may be overly regularized making it hard for a GNN model to distinguish them. However, at the B-AFG level the overall trend of coarsening, while far less clear is noticeably more consistent. Ranging between 85.2-90.1% as compared to 81.0-92.3% at the C-CFG level. Furthermore, we also observe that maximal coarsening also decreases performance similarly for both methods.

When evaluating classwise F1 scores at the C-CFG and B-AFG levels, shown in Table II, we observe similar trends as in panels *b* and *c*, respectively. As mentioned prior, we also observe under consistent under performance in the benign class (approximately 2-3%) across varying  $r$  values and the baseline. Overall, these trends suggest that class specific inference is not extremely impacted by coarsening, thus addressing the inference aspect of **RQ3**.

Lastly, inference evaluation for the proposed Meta-Coarsening approach should be viewed and considered with respect to its intended purpose; to provide comprehensive supporting evidence of model performance towards our explainability results. The overall goal is not for our Meta-Coarsening approach to be used strictly for inference but to support malware detection and assembly level explainability.

#### D. Explainability Evaluation

While typical inference performance metrics are computed using the entire test set, explainability metrics require evalua-

tion using correctly predicted test samples only. This is due to the focus of understanding the phenomenon related to an aspect of class decidability rather than evaluating the decidability of the GNN model itself [2]. Therefore, we only consider correctly predicted test samples when computing explainability metrics.

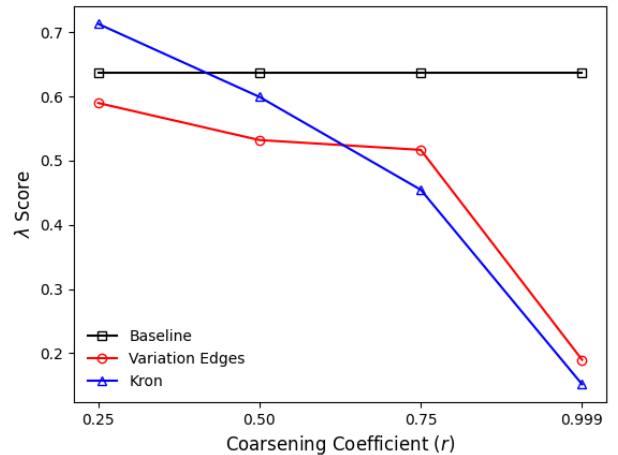


Fig. 7.  $\lambda$  scores.

In terms of explainability, shown in Table III and summarized in Fig. 7, we observe that Kron with a coarsening  $r$  value of 0.25 achieves the highest  $\lambda$  score of **0.713**, indicating strong explainability agreement between the C-CFG and B-AFG. However, fully interpreting this score requires further assessing the fidelity components ( $fid_+$  and  $fid_-$ ) of the respective characterization scores. Most importantly, we observe that  $fid_+$  values, shown in Fig. 8, are the main result of this characterization difference from 0.675 at the C-CFG level to 0.030 at the B-AFG level. These  $fid_+$  scores strongly suggest that our selected C-CFG subgraphs are *necessary*. Meaning that their removal causes misclassification. Furthermore, low

TABLE III  
EXPLAINABILITY RESULTS. COMBINED MALICIOUS AND BENIGN CLASSES DENOTED WITH *All*.

Method	$r$	Level	Explainability						
			Average Characterization				Average Fidelity <sub>All</sub>		$\beta$
			$\lambda_{All}$	<i>All</i>	Benign	Malicious	Minus	Plus	
Baseline	0	CFG	0.637	0.724	0.805	0.587	0.106	0.621	1
		B-AFG		0.087	0.029	0.133	0.031	0.046	<b>0</b>
Variation Edges	0.25	C-CFG	0.590	0.692	0.751	0.515	0.153	0.594	1
		B-AFG		0.102	0.040	0.151	0.047	0.054	<b>0</b>
	0.5	C-CFG	0.532	0.684	0.758	0.560	0.106	0.567	1
		B-AFG		0.152	0.106	0.185	0.096	0.084	<b>0</b>
	0.75	C-CFG	0.517	0.675	0.761	0.518	0.154	0.576	1
		B-AFG		0.158	0.167	0.149	0.111	0.091	<b>0</b>
	0.999	C-CFG	0.190	0.501	0.284	0.000	0.455	0.471	1
		B-AFG		0.312	0.349	0.137	0.301	0.216	<b>0</b>
Kron	0.25	C-CFG	<b>0.713</b>	0.770	0.790	0.722	0.083	0.675	1
		B-AFG		0.057	0.049	0.063	0.042	0.030	<b>0</b>
	0.5	C-CFG	0.599	0.707	0.834	0.565	0.066	0.586	1
		B-AFG		0.107	0.080	0.128	0.122	0.060	<b>0</b>
	0.75	C-CFG	0.455	0.634	0.730	0.480	0.123	0.509	1
		B-AFG		0.179	0.195	0.163	0.098	0.104	<b>0</b>
	0.999	C-CFG	0.151	0.400	0.229	0.007	0.505	0.361	1
		B-AFG		0.249	0.327	0.164	0.167	0.155	<b>0</b>

values at the B-AFG level indicate that it is extremely difficult to remove a subgraph to force misclassification, albeit at a different but highly related level. A low score at the B-AFG level also serves to confirm the prior  $fid_+$  score used to derive the B-AFG.

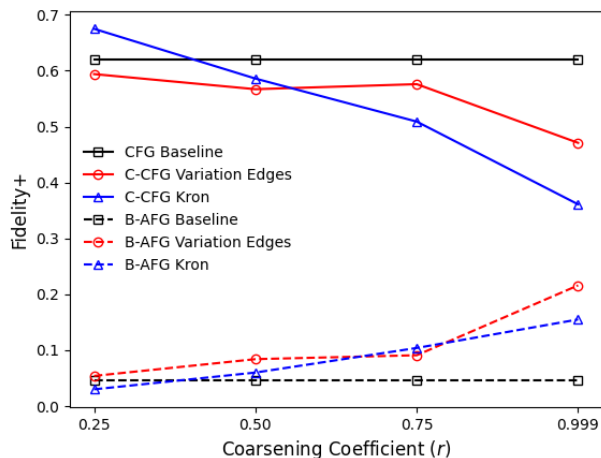


Fig. 8.  $fid_+$  results at (C-)CFG and B-AFG levels.

Furthermore, we also observe a very small increase in  $fid_-$  values from 0.083 at the C-CFG level to 0.042 at the B-AFG level, shown in Fig. 9. These  $fid_-$  scores strongly indicate that our selected subgraphs, at both levels, are highly *sufficient*. Meaning that they provide the same correct predictions.

Overall, these findings indicate that only  $fid_+$  is strongly impacted by our Meta-Coarsening method. Further evidence of our Meta-Coarsening approach to provide strong characterization capability for malicious and benign phenomenon, thus addressing **RQ2**.

Furthermore, as coarsening is increased we generally observe a decrease in  $\lambda$  score. This aligns with our intuition since coars-

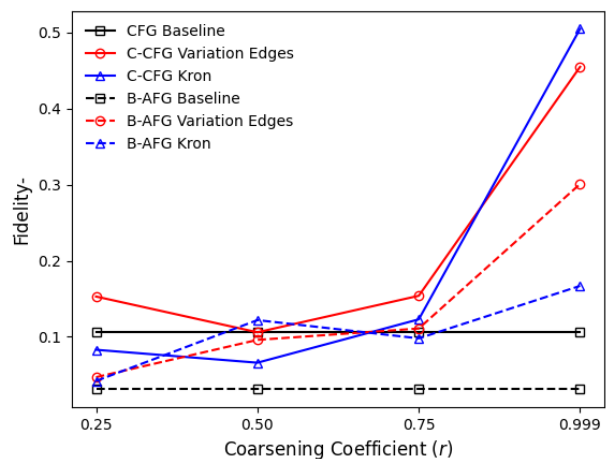


Fig. 9.  $fid_-$  results at (C-)CFG and B-AFG levels.

ening focus on contracting nodes with respect to graph structure rather than importance. This leads to reduced differentiability since important and unimportant nodes become non-separable when contracted into supernodes. Unlike inference, this naturally harms explainability since separability is an important aspect of deriving post-hoc explainability. Additionally, we also observe significant differences in classwise  $\lambda$  and characterization scores, shown in Table III. Specifically, a baseline **31.2** point  $\lambda$  difference exists between benign and malicious classes. This suggests that the malicious class is generally much less explainable than the benign class overall in our setting. Furthermore, when coarsening is applied, we observe that explainability for both classes degrades with respect to the baseline case while maintaining the prior difference. The exception being Kron with  $r$  of 0.25 that interestingly boosts malicious explainability over the baseline. Furthermore, when coarsening is maximal explainability is reduced for both classes

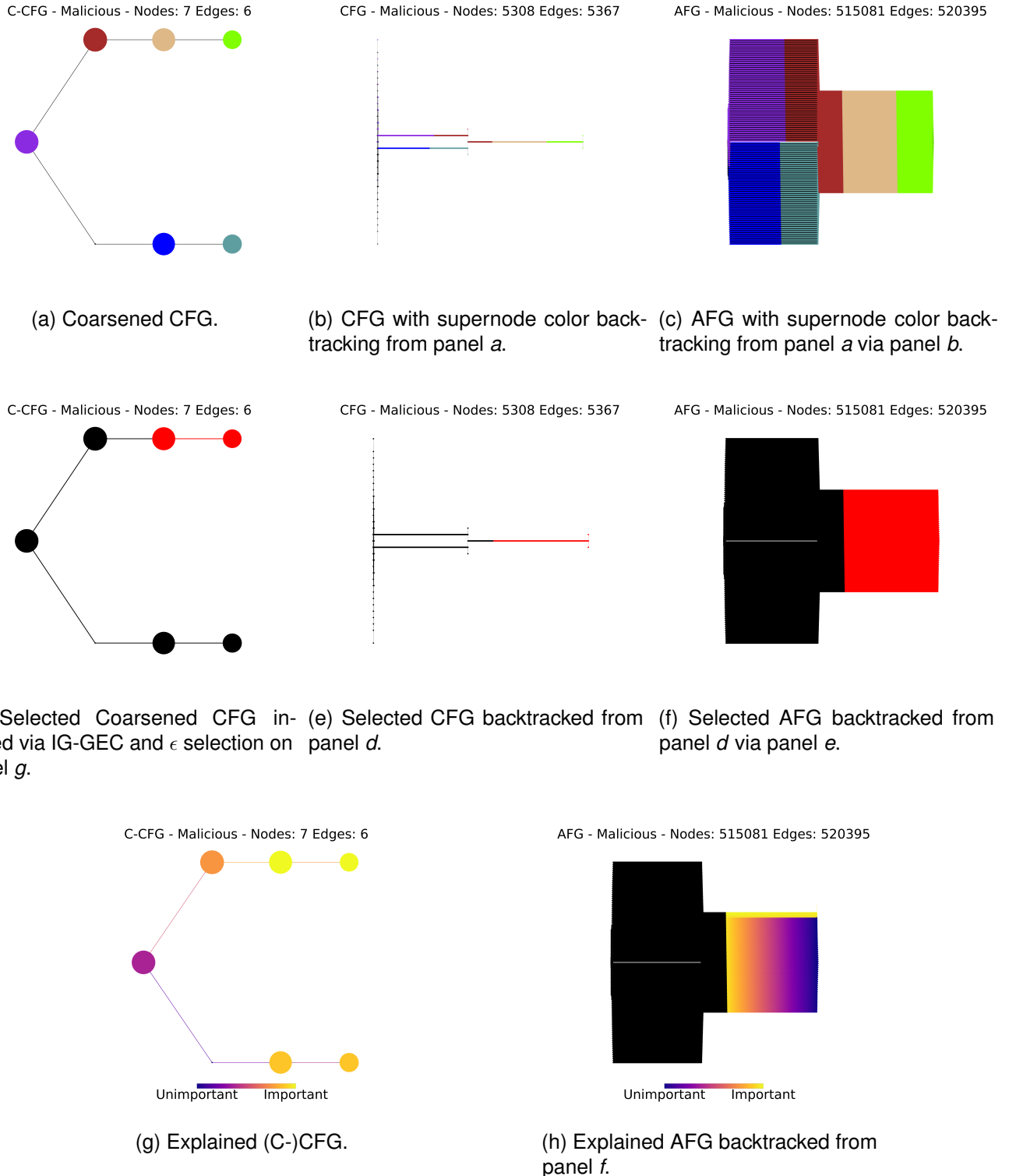


Fig. 10. Plots of coarsened, selected, and explained malicious graph at the (C-)CFG and (B-)AFG levels with Kron coarsening ( $r = 0.999$ ), IG explainer,  $\tau = \text{TES}$ , and  $\epsilon = 10\%$ . Node size in all panels are representative of the total number of instructions that belong to it. Hot and cool color gradients (yellow to purple) in panels *g* and *h* represent explained importance from high to low, respectively.

below zero indicating extremely poor explainability. These observations help address **RQ3** in terms of explainability.

Most importantly, we also observe that the  $\beta$  indicator is maximal for all (C-)CFGs and minimal for all B-AFGs, shown

in Table III. This means that there is no ambiguity with respect to the explanations at the B-AFG level since they are made at the assembly instruction level compared to (C-)CFG, where there is always ambiguity at the basic block level. **This finding**

is extremely important as it empirically highlights a major limitation of CFG or similar (e.g., FCG) with respect to explanation granularity that our proposed approach addresses.

Lastly, we visualize an end-to-end test sample using our Meta-Coarsening approach, shown in Fig. 10, where we consider Kron with  $r = 0.999$  to assist with visualization. In all panels, the size of nodes indicate the number of instructions present. In panel *a*, the C-CFG is visualized with nodes of differing colors representing the supernodes backtracked onto the CFG in panel *b* and B-AFG in panel *c*. This shows that the coarsened supernode mapping is consistent across the various levels. Next, in panel *g*, we visualize the C-CFG explainability. Here, yellow nodes are more important compared to orange and purple nodes, respectively. In panel *d*, we visualize the top selected nodes using the explanation from panel *g*. We also visualize the backtracking from the CFG level onto the B-AFG level in panels *e* and *f*, respectively. This also demonstrates that selection mapping is consistent across the various levels. Lastly, in panel *h*, we visualize the explainability at the B-AFG level. Here, we observe different regions, some with smooth gradients indicating their importance.

## VI. DISCUSSION AND LIMITATIONS

With respect to **RQ1**, the application of coarsening is beneficial for inference performance using specific coarsening methods and coefficients, i.e. Variation Edges and Kron with  $r$  values of 0.25 and 0.75, respectively.

Regarding **RQ2**, the impact of our proposed Meta-Coarsening approach can improve explainability at low to moderate coarsening levels. Specifically, we recognize that our  $\lambda$  score, that considers the dependency between (C-)CFG and B-AFG levels, shows a large increase over the baseline case for low coarsening with Kron specifically. However, high to maximal coarsening tends to diminish explainability. Furthermore, our  $\beta$  score empirically demonstrates that *instruction level explainability is not possible at the (C-)CFG level with GNNs, necessitating our novel application of AFG and Meta-Coarsening approach*.

With respect to **RQ3**, we find there are large differences between both malicious and benign classes. Specifically, we observe that the benign class is more explainable than predictable compared to the malicious class and vice versa. Further research is needed to understand exactly why this is the case, though we provide some initial intuition in our work.

1) *Limitations*: Lastly, several limitations of our work exist. Specifically, it is unclear if our method will generalize to all other types of binary samples. However, this is extremely challenging to address without additional datasets that contain malicious and benign *binary executable samples* specifically for Windows PE x86. Furthermore, some settings may contain graphs with much larger samples than we use here. Though, we do provide a framework for working with them by controlling for  $r$  and  $\epsilon$ . Additionally, our coarsening approaches are largely deterministic and likely much more expensive than state-of-the-art neural coarsening methods. However, to the best of our knowledge, there are no easily implementable libraries

available for neural coarsening. If this were the case, then fast coarsening of large AFG graphs might be feasible. While not part of our work, our theoretical *end-to-end* pipeline necessitates a generation phase that in some cases incurs a very large upfront dynamic generation cost in practice. Future work could consider using statically generated samples CFGs or FCGs. Lastly, we do not consider adversarial evasion techniques, zero days, or metamorphic code. Adversarial training, and careful instruction perturbation might help towards some of these issues.

2) *Ethical Considerations*: In our work, we primarily focus on explainability for the purpose of assisting defenders to characterize malware. However, even though our overall goal is defensive in nature, it could be used to support adversaries. Theoretically, an adversary could use our work to evade detection of our method via the removal or perturbation of highly characterized malicious subgraphs. Though it is unclear as to if this would preserve the overall malicious nature of such programs. While we do not explore this scenario, we expect that methods such as adversarial training could be used as a potential mitigation. Furthermore, we reasonably expect that a much larger collection of data, specifically Windows PE x86 executable samples, not generally available to the scientific or public communities, is needed to realize the evasion attack assisted by our method.

## VII. CONCLUSION

In our work, we propose a novel approach, Meta-Coarsening, that can provide granular assembly instruction level explanations for malware detection using GNNs. To the best of our knowledge, we are the first to propose a GNN-based technique that is able to learn and explain at varying levels of program flow down to the assembly level. Most importantly, our proposed approach is capable of operating on large graphs that would otherwise be computationally demanding in practice. By applying coarsening-based methods, such as Kron and Variation Edges, our approach maintains computational efficiency while ensuring performant inference and strong explainability. Furthermore, to make our approach practical in various settings different hyperparameters such as  $\epsilon$ ,  $r$  can be used to control the size of graphs. Additionally, we also provide a well defined explanation selection strategy,  $\pi$  and  $\tau$  to enhance explainability.

Our results show that at specific levels coarsening can improve inference and explainability. Furthermore, our results illustrate an important finding. That benign samples tend to be much more explainable than malicious samples in our setting. This and other explainability results are supported through the use of the strongest available explanation metric, characterization score, that considers both sufficiency and necessity of explanations not considered in other works.

We conclude that our work has accomplished its goal of providing assembly level explanations over AFG graphs through GNNs. It is our hope that our work serves as inspiration for others to evaluate large scale malware detection explainability and can assist defenders against malware through our approach.

## REFERENCES

- [1] T. Bilot, N. El Madhoun, K. Al Agha, and A. Zouaoui, "A survey on malware detection with graph representation learning," vol. 56, no. 11, pp. 1–36. [Online]. Available: <https://dl.acm.org/doi/10.1145/3664649>
- [2] K. Amara, R. Ying, Z. Zhang, Z. Han, Y. Shan, U. Brandes, S. Schemm, and C. Zhang, "GraphFramEx: Towards systematic evaluation of explainability methods for graph neural networks," *arXiv preprint*, no. arXiv:2206.09677, 2024. [Online]. Available: <http://arxiv.org/abs/2206.09677>
- [3] B. Anderson, D. Quist, J. Neil, C. Storlie, and T. Lane, "Graph-based malware detection using dynamic analysis," *Journal in Computer Virology*, vol. 7, no. 4, pp. 247–258, Nov. 2011. [Online]. Available: <https://doi.org/10.1007/s11416-011-0152-x>
- [4] N. Runwal, R. M. Low, and M. Stamp, "Opcode graph similarity and metamorphic detection," *Journal in Computer Virology*, vol. 8, no. 1, pp. 37–52, May 2012. [Online]. Available: <https://doi.org/10.1007/s11416-012-0160-5>
- [5] H. Hashemi, A. Azmoodeh, A. Hamzeh, and S. Hashemi, "Graph embedding as a new approach for unknown malware detection," *Journal of Computer Virology and Hacking Techniques*, vol. 13, no. 3, pp. 153–166, Aug. 2017. [Online]. Available: <https://doi.org/10.1007/s11416-016-0278-y>
- [6] A. Khalilian, A. Nourazar, M. Vahidi-Asl, and H. Haghighi, "G3md: Mining frequent opcode sub-graphs for metamorphic malware detection of existing families," vol. 112, pp. 15–33. [Online]. Available: <https://www.sciencedirect.com/science/article/pii/S0957417418303580>
- [7] A. G. Kakisim, M. Nar, and I. Sogukpinar, "Metamorphic malware identification using engine-specific patterns based on co-opcode graphs," *Computer Standards & Interfaces*, vol. 71, p. 103443, Aug. 2020. [Online]. Available: <https://www.sciencedirect.com/science/article/pii/S0920548919302685>
- [8] F. K. Wai and V. L. L. Thing, "Clustering based opcode graph generation for malware variant detection," in *2021 18th International Conference on Privacy, Security and Trust (PST)*. Los Alamitos, CA, USA: IEEE Computer Society, Dec. 2021, pp. 1–11. [Online]. Available: <https://doi.ieeecomputersociety.org/10.1109/PST52912.2021.9647814>
- [9] A. G. Kakisim, S. Gulmez, and I. Sogukpinar, "Sequential opcode embedding-based malware detection method," *Computers & Electrical Engineering*, vol. 98, p. 107703, 2022. [Online]. Available: <https://www.sciencedirect.com/science/article/pii/S0045790622000210>
- [10] H. Shokouhinejad, G. Higgins, R. Razavi-Far, H. Mohammadian, and A. A. Ghorbani, "On the consistency of gnn explanations for malware detection," *Information Sciences*, vol. 721, p. 122603, 2025. [Online]. Available: <https://www.sciencedirect.com/science/article/pii/S0020025525007364>
- [11] J. D. Herath, P. P. Wakodikar, P. Yang, and G. Yan, "CFGExplainer: Explaining graph neural network-based malware classification from control flow graphs," in *2022 52nd Annual IEEE/IFIP International Conference on Dependable Systems and Networks (DSN)*, pp. 172–184, ISSN: 2158-3927. [Online]. Available: <https://ieeexplore.ieee.org/document/9833560>
- [12] H. Shokouhinejad, R. Razavi-Far, G. Higgins, and A. A. Ghorbani, "Dual explanations via subgraph matching for malware detection," *arxiv preprint*, no. arXiv:2504.20904. [Online]. Available: <http://arxiv.org/abs/2504.20904>
- [13] H. Shokouhinejad, R. Razavi-Far, H. Mohammadian, M. Rabbani, S. Ansong, G. Higgins, and A. A. Ghorbani, "Recent advances in malware detection: Graph learning and explainability," *arXiv preprint*, no. arXiv:2502.10556, 2025. [Online]. Available: <http://arxiv.org/abs/2502.10556>
- [14] Karl-Bridge-Microsoft, "PE Format - Win32 apps." [Online]. Available: <https://learn.microsoft.com/en-us/windows/win32/debug/pe-format>
- [15] Y. Shoshitaishvili, R. Wang, C. Salls, N. Stephens, M. Polino, A. Dutcher, J. Grosen, S. Feng, C. Hauser, C. Kruegel, and G. Vigna, "Sok: (state of) the art of war: Offensive techniques in binary analysis," in *IEEE Symposium on Security and Privacy*, 2016.
- [16] N. Stephens, J. Grosen, C. Salls, A. Dutcher, R. Wang, J. Corbetta, Y. Shoshitaishvili, C. Kruegel, and G. Vigna, "Driller: Augmenting fuzzing through selective symbolic execution," in *NDSS*, 2016.
- [17] Y. Shoshitaishvili, R. Wang, C. Hauser, C. Kruegel, and G. Vigna, "Firmalce - automatic detection of authentication bypass vulnerabilities in binary firmware," in *NDSS*, 2015.
- [18] A. Loukas, "Graph reduction with spectral and cut guarantees," *Journal of Machine Learning Research*, vol. 20, no. 116, pp. 1–42, 2019. [Online]. Available: <http://jmlr.org/papers/v20/18-680.html>
- [19] qemu, "capstone/include/capstone/x86.h at master · qemu/capstone," <https://github.com/qemu/capstone/blob/master/include/capstone/x86.h>
- [20] G.-A. Iosif, "Dikedataset," <https://github.com/iosifache/DikeDataset>, 2021, accessed on February 27, 2024.
- [21] Practical Security Analytics LLC, "Pe malware machine learning dataset," <https://practicalsecurityanalytics.com/pe-malware-machine-learning-dataset/>, 2024, accessed: 2024-08-06.
- [22] T. N. Kipf and M. Welling, "Semi-supervised classification with graph convolutional networks," *arXiv preprint*, no. arXiv:1609.02907, 2017. [Online]. Available: <http://arxiv.org/abs/1609.02907>
- [23] N. Kokhlikyan, V. Miglani, M. Martin, E. Wang, B. Alsallakh, J. Reynolds, A. Melnikov, N. Kliushkina, C. Araya, S. Yan, and O. Reblitz-Richardson, "Captum: A unified and generic model interpretability library for pytorch," *arXiv preprint*, no. arXiv:2009.07896, 2020. [Online]. Available: <https://arxiv.org/abs/2009.07896>
- [24] Z. Ying, D. Bourgeois, J. You, M. Zitnik, and J. Leskovec, "Gnnexplainer: Generating explanations for graph neural networks," *Advances in Neural Information Processing Systems (NIPS)*, vol. 32, 2019.
- [25] D. Luo, W. Cheng, D. Xu, W. Yu, B. Zong, H. Chen, and X. Zhang, "Parameterized explainer for graph neural network," in *34th International Conference on Neural Information Processing Systems*, 2020.
- [26] D. I. Shuman, M. J. Faraji, and P. Vandergheynst, "A Multiscale Pyramid Transform for Graph Signals," *IEEE Transactions on Signal Processing*, vol. 64, no. 8, pp. 2119–2134, Apr. 2016. [Online]. Available: <https://ieeexplore.ieee.org/document/7366599/>
- [27] M. Fey and J. E. Lenssen, "Fast graph representation learning with PyTorch Geometric," in *ICLR Workshop on Representation Learning on Graphs and Manifolds*, 2019.
- [28] M. Fey, J. Sunil, A. Nitta, R. Puri, M. Shah, B. Stojanovič, R. Bendias, B. Alexandria, V. Kocijan, Z. Zhang, X. He, J. E. Lenssen, and J. Leskovec, "PyG 2.0: Scalable learning on real world graphs," in *Temporal Graph Learning Workshop @ KDD*, 2025.
- [29] A. A. Hagberg, D. A. Schult, and P. J. Swart, "Exploring network structure, dynamics, and function using networkx," in *Proceedings of the 7th Python in Science Conference*, G. Varoquaux, T. Vaught, and J. Millman, Eds., Pasadena, CA USA, 2008, pp. 11 – 15.

## APPENDIX

## A. Explainer Comparison and Characterization Curve Analysis

Here, we provide additional explainability analysis and comparison of IG with Guided Back Propagation (GBP) and Saliency (SAL) explainers from the Captum library [23]. Specifically, at each explanation level we compute the impact of sparsity on characterization accuracy. However, at the AFG level all explanations are derived from IG output to form a consistent comparison.

When examining general explanation trends over all experiments, we observe that in many cases at the (C-)CFG level, shown in Figures 11 panel *a*, 12 panel *e*, and 13 panels *a*, *c*, *e* that at IG, GBP, and SAL perform best, from high to low, respectively. However, in some cases when using Variation Edges, SAL tends to outperform other explainers, shown in Figure 12 panels *c* and *g*. Furthermore, at the B-AFG level we generally observe similar performance across explainers, shown in Figures 11 panel *b*, 12 panel *b*, 13 panel *b*, *d*, *f*, and 13 *b*, *d*, *f*. However, in some cases we also observe the previous trend of IG, GBP, and SAL from high to low, respectively, shown in Figures 12 panel 13 all panels *h*, when coarsening is maximal.



Fig. 11. Characterization accuracy curves for **Baseline**, i.e., no coarsening, with  $r = 0$ .

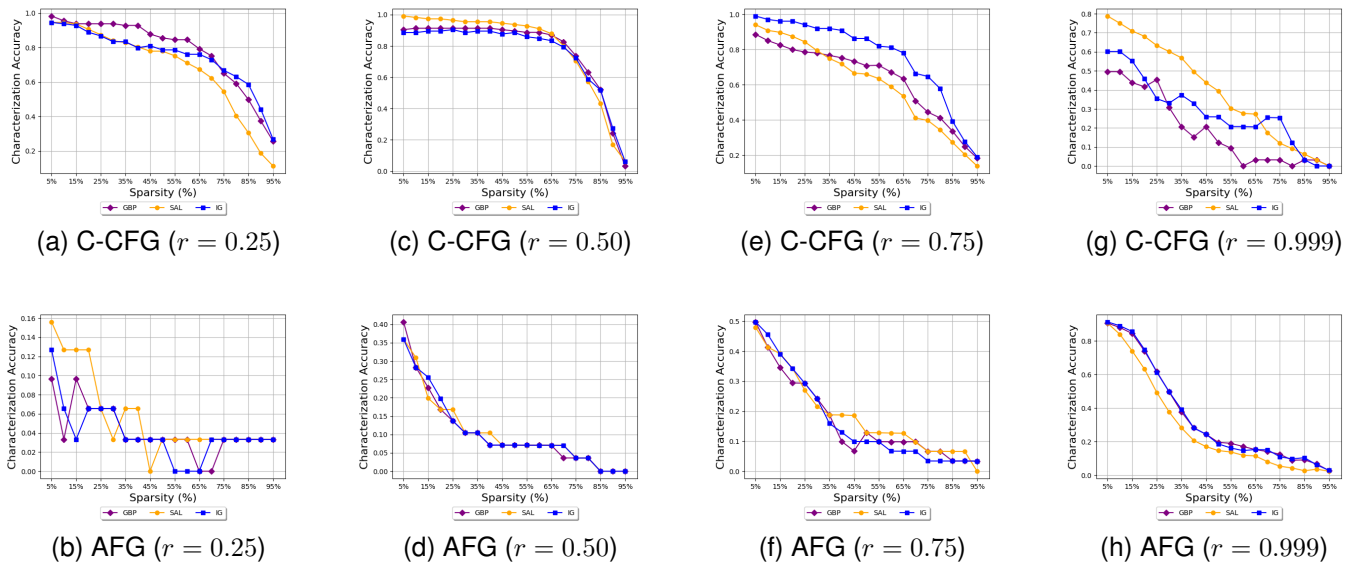


Fig. 12. Characterization accuracy curves for **Variation Edges** with  $r \in \{0.25, 0.5, 0.75, 0.999\}$ .

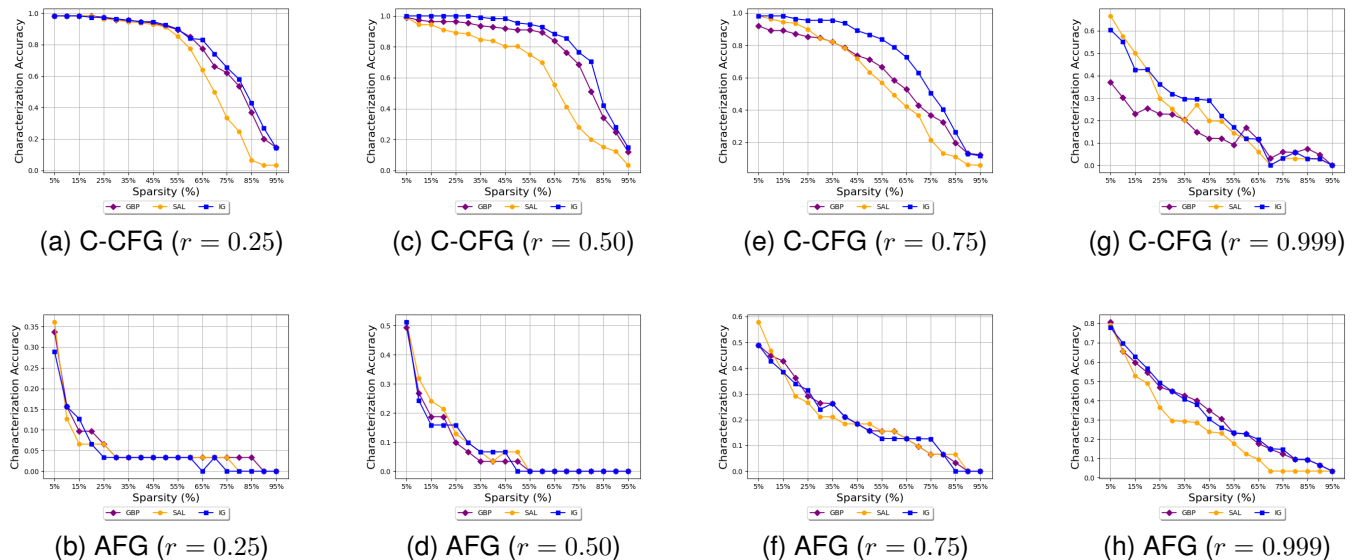


Fig. 13. Characterization accuracy curves for **Kron** with  $r \in \{0.25, 0.5, 0.75, 0.999\}$ .